CARTILAGE
April-June 2022: 1–13
© The Author(s) 2022
DOI: 10.1177/19476035221098165
journals.sagepub.com/home/CAR
SAGE

Early Emergent and Progressive Aberrant Subchondral Bone Remodeling Coupled with Aggravated Cartilage Degeneration in Developmental Dysplasia of the Hip

Teng Ye[1], Feng Xue[1], Hai Hu[1], Zihao He[2], Minqi Wang[3], Zhifeng Yu[2], Bizeng Zhao[1], and Linyang Chu[1]

Abstract

Objective. Developmental dysplasia of the hip (DDH) is the most common skeletal development in children and could result in secondary osteoarthritis. This study aims to clarify the alternations of subchondral trabecular bone remodeling and microstructural properties during the development of DDH, and the potential influence of these alternations on the overlying cartilage degeneration and DDH progression. *Design.* Traditional straight-leg swaddling method was adopted to establish DDH model in newborn Sprague Dawley rats. Hip joint specimens from normal or DDH rats were used. Typical features of DDH in radiological examination were observed by x-ray analysis. Micro–computed tomography analysis was applied to evaluate the microstructural properties of subchondral bone at postnatal weeks 2, 4, and 6. Histological and immunohistochemical analyses were adopted to appraise subchondral bone remodeling activity and cartilage degeneration. The associations among subchondral bone, articular cartilage, and DDH severity were analyzed via multiple linear regression analysis. *Results.* Compared with control group, the subchondral bone in DDH group displayed a gradual trend of deteriorated microstructure and worsening biomechanical properties along with aberrant bone remodeling, which might be responsible for the inhibition of stress transmission from the articular cartilage to the subchondral bone and thus leading to the cartilage degeneration and accelerated DDH progression. *Conclusions.* Our findings indicate that alternations of subchondral trabecular bone in a time-dependent manner could contribute to the DDH progression and the amelioration on subchondral bone might be a favorable therapeutic candidate for DDH.

Keywords

subchondral bone microstructure, bone remodeling, developmental dysplasia of the hip, cartilage degeneration, biomechanics

Introduction

Developmental dysplasia of the hip (DDH) is a common congenital abnormality, which impairs the acetabulum and occasionally the proximal femur over a lifetime.[1,2] The hip instability caused by DDH can lead to inhomogeneous stress distribution and raise the risk of chondral degeneration and secondary osteoarthritis (OA).[3-5] A cross-section survey revealed that the prevalence of DDH was 1.52% among Chinese adults; the total medical costs pose a heavy financial burden on the Chinese medical system.[6] For DDH patients, if they cannot be detected early and treated appropriately, most of them will develop serious hip OA and require total hip replacement (THA).[7-9] The best way to prevent hip dysplasia from progressing to secondary OA is to diagnose it as soon as possible and restore the natural anatomical hip structure before the cartilage degeneration becomes irreversible.[10] Therefore, the key issue is to illustrate the specific progress and the underlying biomechanisms in the development of DDH.

Recently, some studies have suggested that microstructural changes in subchondral trabecular bone might be a crucial factor for the development of primary OA using imaging technologies, such as the micro–computed tomography (μCT).[11-14] Meanwhile, Liu *et al.*[15] found that the subchondral bone biomechanical properties in OA patients extracted by micro–finite element analysis (μFEA) were closely related with the variations of subchondral bone microstructure and had a profound effect on OA progression. We have formerly illustrated that the changes in subchondral bone could bring

about the accelerated OA progression while OA co-occurred with osteoporosis in the same individuals.[16] However, there are few studies about whether these changes could affect the DDH ongoing, which needs to be further clarified. Moreover, it is not clear whether the onset of DDH is initiated in cartilage or subchondral bone. In our previous study, we have compared structural and biomechanical properties of subchondral trabecular bone and their relevance with cartilage degradation between advanced DDH patients and primary OA patients. Our findings revealed that DDH patients had deteriorating microstructures and inferior biomechanical properties of subchondral trabecular bone, which might have a connection with cartilage damage.[17] Nevertheless, our previous study merely analyzed patients with advanced symptoms of DDH and did not observe the dynamic changes of subchondral trabecular bone remodeling, microstructural properties, and their relationship with cartilage degeneration during the whole development of DDH, which so far remains unknown. Solving these above-mentioned problems will enable us to better understand the biomechanical changes underlying the pathogenesis of DDH and establish a subchondral trabecular bone–related targeting treatment.

In this study, we performed a straight-leg swaddling model on Sprague Dawley rats to investigate the alternations in subchondral trabecular bone and their relationships with cartilage degeneration in the development of DDH. We aimed to clarify the changes of subchondral bone remodeling and microstructural properties in the time dimension during the development of DDH and explore the effect of these changes on the overlying cartilage damage. We hypothesize that during the DDH progress, the subchondral bone might gradually undergo aberrant bone remodeling and cause the deterioration of microstructure and biomechanical properties, thereby impairing normal hip joint structure and finally leading to severe DDH symptoms.

Methods

Animals and DDH Model

A total amount of 48 male neonatal Sprague Dawley rats (~5 g) were used in the present study. The experimental procedures relating to rats were approved by the Institutional Animal Care and Use Committee (IACUC) of our hospital (approval code: SYXK [Shanghai, China] 2020-0072). The newborn rats were kept at following environment: temperature 20°C~22°C, relative humidity 45%~65%, 12 hours/12 hours light/dark cycle at a specific pathogen-free facility. The rats were randomly distributed to DDH model group ($n = 24$) or control group ($n = 24$) by a randomization table, which was blinded to avoid the bias of this study. After that, rats in separate cages were provided with general food and water. As is shown in **Figure 1A**, the DDH model was induced by a straight-leg swaddling method, which involved fixation of the hip and knee with medical tapes at the positions of hip adduction and extension for postnatal 10 days as previously described.[18,19] Rats in control group received no interventions. Subsequently, 8 rats from the DDH group and 8 rats from the control group were randomly selected and sequentially euthanized under the overdose of pentobarbital sodium at postnatal weeks 2, 4, and 6. At each time point, the rats were subjected to the x-ray analysis immediately after killing, and the whole pelvises containing complete acetabulum and femoral heads were isolated for further analysis (**Fig. 1A** and **B**). The operations were conducted in compliance with the double-blind principle.

X-Ray Analysis

High-resolution radiographs of the standard ventrodorsal hip extended view (SVDV) of pelvis in rats were taken at postnatal weeks 2, 4, and 6, using an x-ray machine (Faxitron X-ray Corporation, USA) with a 3-second exposure time. Several measurements were carried out assessing the extent of hip joint displacement as reported before, including acetabular index (AI), lateral center-edge angle (LCE angle), femoral coverage percent (FC percent), and distraction index (DI).[20] Briefly, AI is described as the angle between a parallel line intersecting the point of the ilium and ischium and another line running from the above-mentioned point to the outer edge of ilium inferior margin. LCE angle is measured by a vertical line and another line connecting the femoral head center with the acetabulum lateral

[1]Department of Orthopedic Surgery, Shanghai Jiao Tong University Affiliated Sixth People's Hospital, Shanghai, China
[2]Shanghai Key Laboratory of Orthopedic Implants, Department of Orthopedic Surgery, Shanghai Ninth People's Hospital, Shanghai Jiao Tong University School of Medicine, Shanghai, China
[3]Department of Bone and Joint Surgery, Renji Hospital, Shanghai Jiaotong University School of Medicine, Shanghai, China

Corresponding Authors:
Zhifeng Yu, Shanghai Key Laboratory of Orthopedic Implants, Department of Orthopedic Surgery, Shanghai Ninth People's Hospital, Shanghai Jiao Tong University School of Medicine, 639# Zhizaoju Road, Shanghai 200011, China.
Email: zfyu@outlook.com

Bizeng Zhao, Department of Orthopedic Surgery, Shanghai Jiao Tong University Affiliated Sixth People's Hospital, 600# Yishan Road, Shanghai 200233, China.
Email: zhaobizeng@aliyun.com

Linyang Chu, Department of Orthopedic Surgery, Shanghai Jiao Tong University Affiliated Sixth People's Hospital, 600# Yishan Road, Shanghai 200233, China.
Email: chulinyang@alumni.sjtu.edu.cn

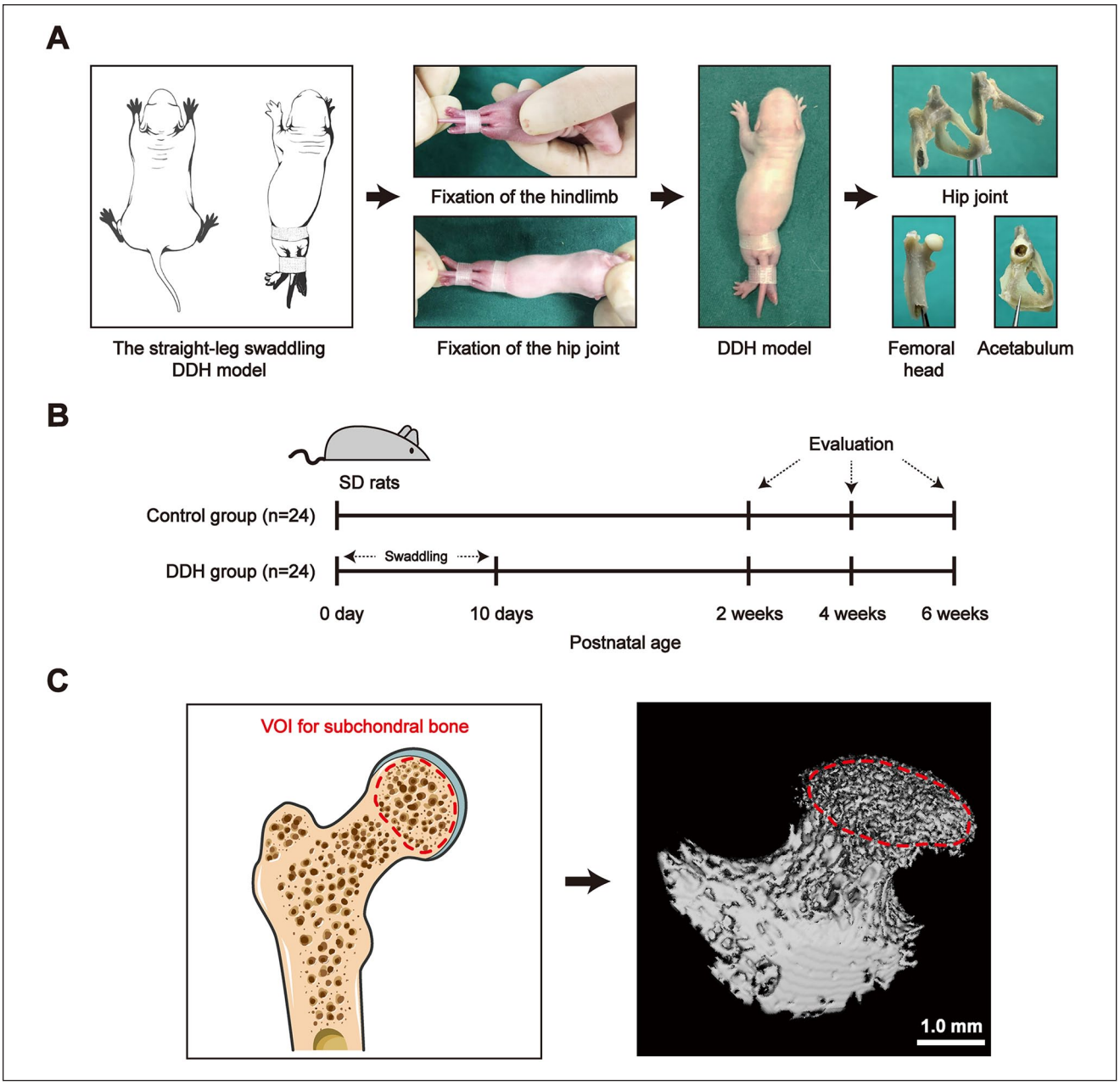

Figure 1. Schematic diagram for the experimental design. (**A**) DDH rats induced by traditional straight-leg swaddling model. (**B**) The hip joints containing femoral head and acetabulum in both groups were collected at different time points for further evaluation. (**C**) Schematic pictures and reconstructed 3D images of the VOI for subchondral trabecular bone (red dashed line). DDH = developmental dysplasia of the hip; VOI = volume of interest.

edge. FC percent is evaluated as the percent of the femoral head covered by the acetabular rim. DI is calculated considering d/r. The d refers to the interval between acetabulum center and femoral head center. The r refers to the radius of the femoral head.

Micro-Computed Tomography Analysis

A high-resolution μCT system (Micro-CT 80; Scanco Medical AG, Switzerland) was employed to scan the whole pelvises and hip joints from both groups from each time point at 10 μm isotropic voxel size. We determined the femoral head subchondral bone as the volume of interest (VOI) using the semiautomatic contouring method, which was extracted by the reconstructed 3-dimensional image (VOI for subchondral bone, **Fig. 1C**). The total bone volume fraction (BV/TV), trabecular bone number (Tb.N), trabecular bone thickness (Tb.Th), and trabecular bone separation (Tb.Sp) were automatically obtained. The structure model index (SMI) was measured using a model based on the type of

structure. The connectivity density (Conn.D.) was defined as a topological parameter of total bone trabecular connections per cubic millimeter.

Histological and Immunohistochemical Analysis

After x-ray analysis and μCT scanning, 4% paraformaldehyde was used for the fixation of all femoral head specimens for 24 hours. Thenceforth, fixed samples were decalcified in 10% EDTA solution for about 3 weeks, followed by the dehydration and paraffin embedding. The embedded samples were cut into serial sections (5 μm) and stained with hematoxylin and eosin (H&E) and Safranin O-Fast Green. The cartilage degeneration level was measured according to the Osteoarthritis Research Society International (OARSI) scoring system.[21] Five sequential sections from each sample were processed and estimated. For Terminal Deoxynucleotidyl Transferase-mediated dUTP Nick-End Labeling (TUNEL) staining, the apoptotic chondrocytes were detected using the In Situ Cell Death Detection Kit, Fluorescein (Sigma-Aldrich) according to the manufacturer's instructions. The number of positively stained cells were calculated by Image-pro Plus software.

Immunohistochemical (IHC) staining was performed to evaluate sections of the decalcified femoral head samples. All sections were deparaffinized and processed with antigen retrieval in citrate buffer. After that, sections were treated with primary antibodies including matrix metalloproteinase-3 (MMP-3; Abcam, UK) and osteocalcin (Abcam, UK) at 4°C overnight. Followed by 3 times of rinse in 0.1 M PBS, sections were incubated with horseradish peroxidase-labeled secondary antibody for 1 hour. Diaminobenzidine was used to develop the substrate color. For the osteoclasts staining, tartrate-resistant acid phosphatase (TRAP) staining was applied according to the protocol of a commercial TRAP staining kit. An optical microscope (Leica Microsystems AG, Germany) was employed to obtain images and the number of positively stained cells were calculated by Image-pro Plus software. In addition, 5 sequential sections in each specimen were stained and 5 areas in each section were evaluated.

Statistical Analysis

Data were processed by the SPSS 19.0 statistical software and presented as mean ± standard deviations (SDs). The comparison of two groups across different time points were conducted using 2-way analysis of variance (ANOVA) and Turkey's test for *post hoc* tests. Furthermore, to explore the correlation of DDH severity and subchondral bone properties in the control and DDH groups, multiple linear regression analyses with microstructure and biomechanical properties of the subchondral bone were performed for the OFA (Orthopedic Foundation for Animals Hip) score, LCE angle, FC percent, percentage of MMP-3$^+$ chondrocytes, and subchondral trabecular bone remodeling activity. For the linear regression analysis, 2-tailed Pearson correlation analyses were adopted. $P < 0.05$ was considered as statistically significant.

Results

Analysis of Macroscopic Observation and Radiography Measurements

Macroscopic observations of the hip joint morphology from control and DDH groups are presented in **Figure 2A**. From the hip general view of the DDH group, the articular capsule of the hip joint became thickened and hypogenetic articular cartilage was unable to be visualized, which proves the usability of our DDH modeling. Conversely, the joint capsule was thin and transparent enough to observe the cartilage in control group. In addition, the shallow acetabulum and flat femoral head were discovered in DDH group at postnatal weeks 2 and 4, which indicated the development of dysplasia hip joint. At postnatal weeks 4 and 6, false acetabulum appeared along with shallow acetabulum. The hip grading of both groups at different time points was classified according to the OFA scoring system,[22] which suggested that the severity of hip deterioration in the DDH group was constantly aggravating over time (**Fig. 2B**).

Radiographic evaluation plays a critical role in the diagnosis of DDH. Among various radiographic measurements, x-ray analysis provides a direct view into the anatomical structure and developmental situation of hip joint. In **Figure 2C**, the anteroposterior pelvic x-ray results demonstrated that the acetabulum fossa was initially formed at postnatal week 4 in control group, which became deeper at postnatal week 6. Meanwhile, the shape of femoral head became fuller during the follow-up period. By contrast, the structure of acetabulum seemed to have disappeared in DDH group and the femoral head showed a dislocation from postnatal weeks 2 to 6. Furthermore, we performed several measurements on x-ray images, including acetabular index (AI), lateral center-edge angle (LCE angle), femoral coverage percent (FC percent), and distraction index (DI), which indicated the femoral head malposition. The AI and DI in DDH group raised dramatically from postnatal weeks 2 to 6, while the AI and DI in control group maintained at a significantly lower degree than the DDH group (**Fig. 2D** and **G**, $P < 0.05$). Interestingly, the center of femoral head in DDH group was located at the outer side of the acetabulum lateral edge, whereas the femoral head center of the control was enfolded by the acetabulum fossa, leading to different LCE angle formation patterns in both groups. Consequently, we defined the LCE angle in the DDH group as a minus value, which was relative to the plus value of LCE angle in the control group. It is obvious that the absolute value of

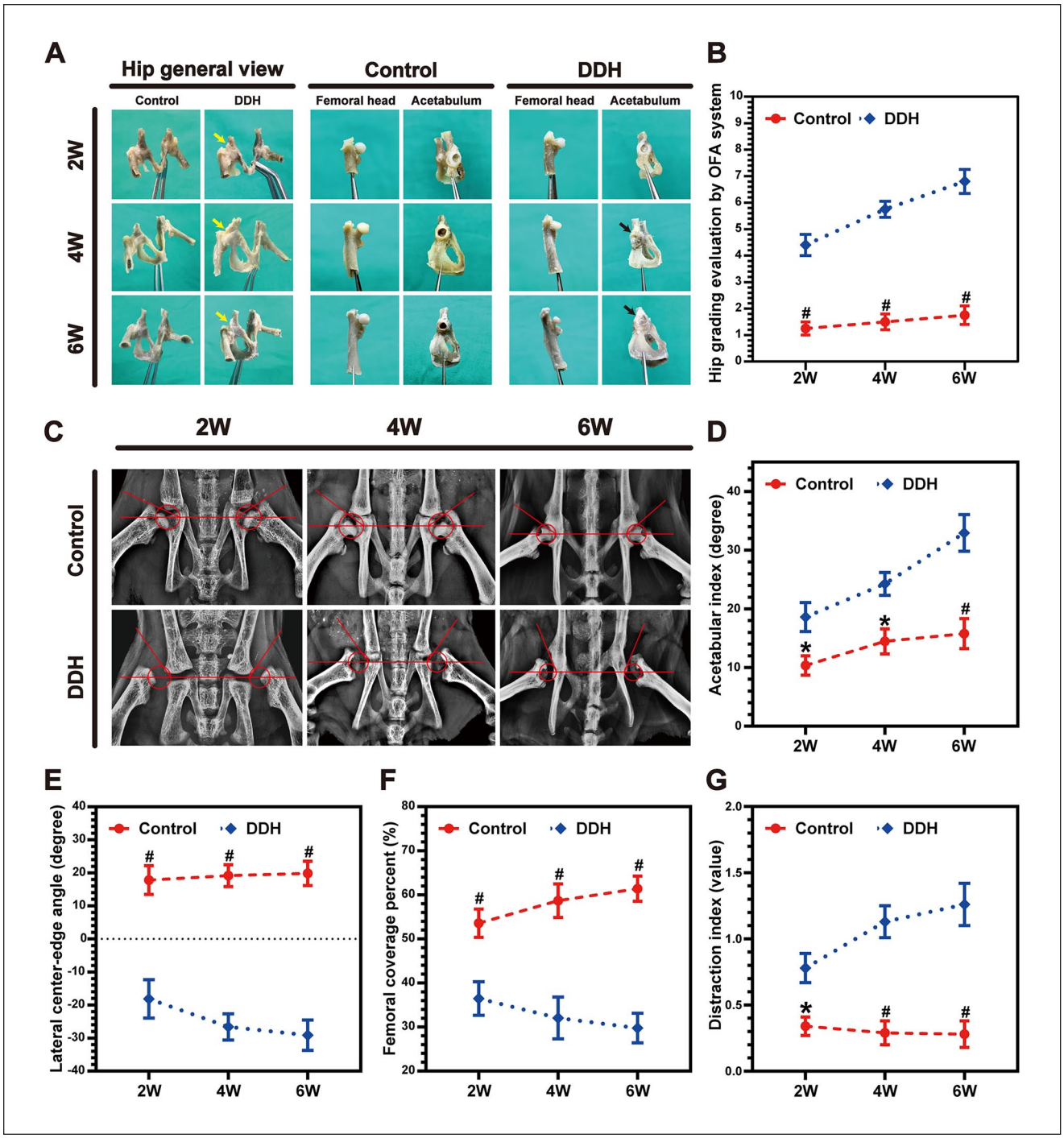

Figure 2. Macroscopic view of the hip joint and analysis of the hip joint x-ray images at different time points. (**A**) General view of the hip joints along with the local view of the dissected femoral head and acetabulum at different time points in the two groups (yellow arrows implying the thickened hip joint capsule, and black arrows implying the false acetabulum). (**B**) Hip grading evaluation by OFA system of both groups at different time points. #$P < 0.01$ compared with DDH group. (**C**) Representative anteroposterior pelvic x-ray images in the two groups at different time points (red solid circle indicating the center of femoral head, the unilateral angle formed by 2 red solid lines referring to the acetabulum index). (**D-G**) Quantitative analysis of the AI, LCE angle, FC percent, and DI in both groups at different time points. *$P < 0.05$ and #$P < 0.01$ compared with DDH group. OFA = Orthopedic Foundation for Animals Hip; DDH = developmental dysplasia of the hip; AI = acetabular index; LCE angle = lateral center-edge angle; FC percent = femoral coverage percent; DI = distraction index.

LCE angle in the DDH group turned out to be increased over time (**Fig. 2E**). The FC percent was remarkably lower in the DDH group than control ($P < 0.05$), which reached the lowest ebb at postnatal week 6 (**Fig. 2F**).

Analysis of Femoral Head Cartilage Degeneration

Histological analysis, TUNEL staining, and IHC analysis were applied to examine the degeneration of femoral head cartilage in both groups. The morphology of cartilage layer was plumper in the control groups than that of DDH groups according to the H&E and Safranin O staining. Moreover, cartilage layer of the DDH groups showed a flat appearance and destructed cartilage surface at week 6 and the transition area of cartilage to subchondral bone seemed much looser (**Fig. 3A** and **B**). The OARSI score results indicated that DDH groups had worse cartilage conditions at weeks 4 and 6 (**Fig. 3E**, $P < 0.01$). To further characterize the cell death in DDH articular cartilage, we performed TUNEL staining on tissue sections. TUNEL staining was significantly increased in DDH cartilage at weeks 4 and 6, which was supported by the quantification of $TUNEL^+$ cells relative to total cell numbers (**Fig. 3C** and **F**). From the IHC staining images and quantification, there were much more $MMP\text{-}3^+$ chondrocytes in the DDH groups than those of control at weeks 4 and 6. The images also revealed that MMP-3 was upregulated in the chondrocytes adjacent to the cartilage surface, which directly suffered abnormal mechanical distribution due to the disarticulation of hip (Fig. 3D and G). A linear regression analysis between the OARSI score and MMP-3-positive chondrocytes ratio (%) revealed that the expression of MMP-3 was highly correlated with the cartilage degeneration in both groups (**Fig. 3H**).

Micro-CT Scanning Analysis

The μCT was performed to visualize the 3D structure of hip joint and femoral head formation at different time points. According to the anteroposterior (AP) view and lateral view of reconstructed μCT images, the shallow acetabulum and femoral head malposition in the DDH group were clearly recognized (**Fig. 4A**). In addition, the bony structure of the femoral head showed a hemisphere-like shape in control group, whereas those in DDH group were irregular and loss of bone (**Fig. 4B**). The femoral head subchondral bone microstructures were extracted by μCT evaluation and presented in **Figure 4C-H**. Compared with the control group, the BV/TV and Conn.D. in DDH group were remarkably lower at postnatal week 2, which further decreased at weeks 4 and 6 (**Fig. 4C** and **D**, $P < 0.05$). The notable morphological characteristics of subchondral bone in both groups were observed as the SMI values in the DDH group were significantly higher, suggesting that the subchondral bone of the DDH group had more scattered trabecula (**Fig. 4E**, $P < 0.05$). Moreover, the DDH group had lower Tb.N and Tb.Th values but higher Tb.Sp, which indicated that the subchondral bone microstructure in DDH group was more deteriorative and dispersed (**Fig. 4F-H**). Generally, the subchondral bone microstructural differences between the two groups became more and more significant over time, which indicated that the subchondral bone appear to suffer aberrant alternations during the continuous progression of DDH while compared with the normal hip joint development.

Analysis of Subchondral Bone Remodeling

The subchondral bone remodeling activity was investigated by immunohistochemistry and presented in **Figure 5**. In DDH groups, there were significantly fewer $osteocalcin^+$ osteoblasts and more $TRAP^+$ osteoclasts in subchondral bone than control at different time points, implying that the abnormal bone resorption activity in DDH groups took a predominant place of subchondral bone remodeling during continuous DDH progression, while the bone formation activity played a major role throughout the normal development in control groups. From the time-course quantitative results in **Figure 5B** and **C**, the bone formation activity in control group kept increasing from weeks 2 to 6, whereas the aberrant bone resorption activity in DDH group became more and more serious.

Multiple Linear Regression Analysis between Subchondral Bone, Cartilage Degeneration, and DDH Severity

As is shown in **Table 1**, the multiple linear regression analysis was employed to illuminate the correlation between subchondral bone microstructural properties and remodeling activity. Because of the very few of $TRAP^+$ osteoclasts in control group, the relevance between TRAP and subchondral bone properties seems to be indistinct. The results of **Table 1** suggested that the subchondral bone formation activity (OCN) was positively correlated with most of the subchondral bone microstructural properties (BV/TV, Conn.D, Tb.N, Tb.Th) and negatively correlated with SMI and Tb.Sp in both groups, whereas the resorption activity (TRAP) displayed a strong association with BV/TV, Conn.D, SMI, Tb.N, and Tb.Sp in DDH group ($r^2 > 0.3$, $P < 0.05$). Moreover, multiple linear regression analysis was also adopted to illuminate the correlation between the subchondral bone microstructural properties and DDH severity (OFA score, LCE angle, FC percent, and MMP-3) in **Table 2**. Evidently, the correlation coefficients for these subchondral bone properties were higher in DDH group, implying that subchondral bone properties acted as a pivotal part

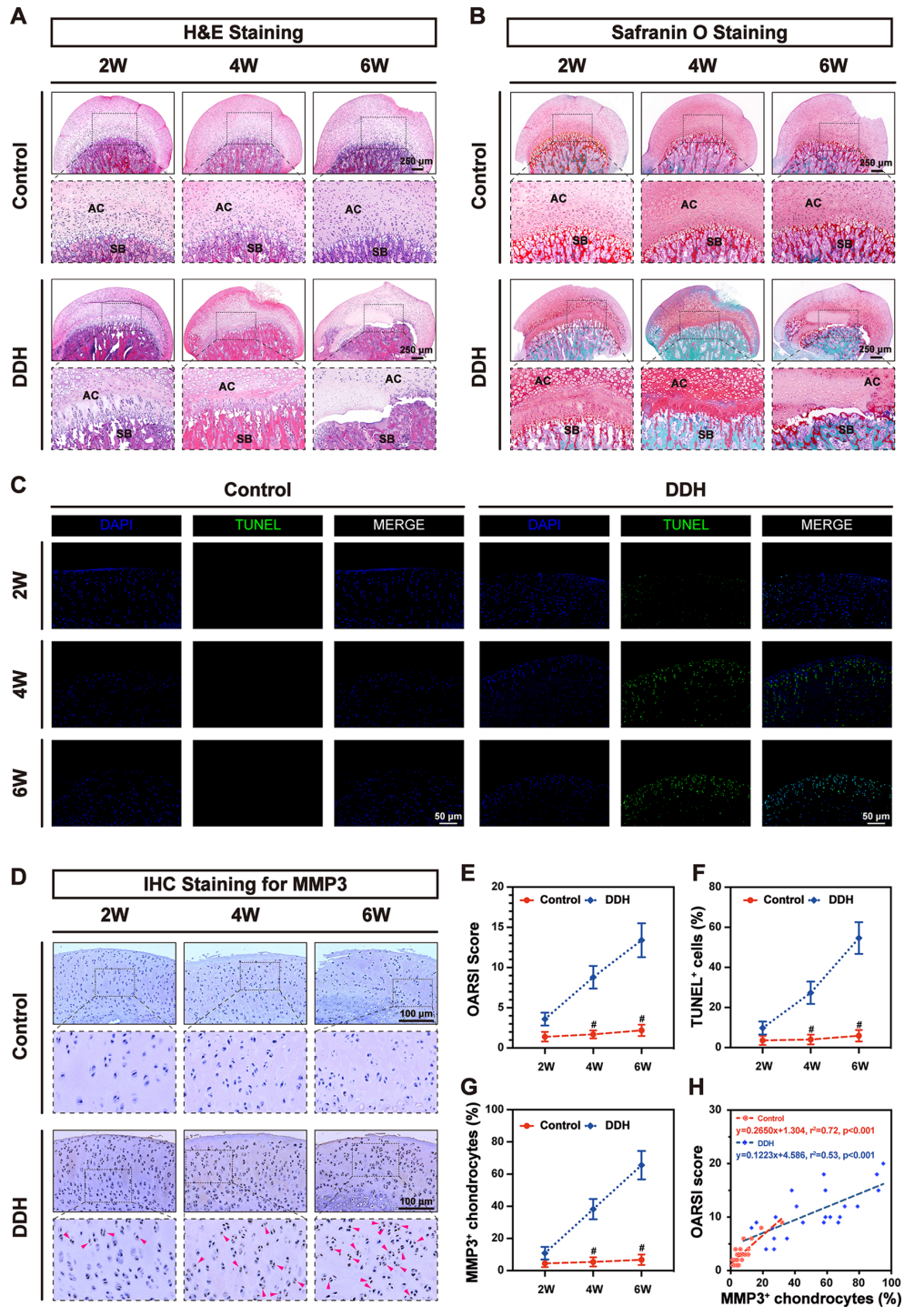

Figure 3. Analysis of the femoral head cartilage at different time points. (**A-B**) Representative images of hematoxylin and eosin staining and Safranin O staining for femoral head in both groups. (**C**) Representative images of TUNEL staining for femoral head chondrocytes in both groups. (**D**) Representative images of IHC staining for matrix metalloproteinase-3 (MMP-3^{+}) chondrocytes in cartilage in both groups (red arrows indicating the MMP-3^{+} chondrocytes). (**E**) Quantitative results of the OARSI score in both groups. (**F**) Quantitative results of the TUNEL^{+} cells ratio (%) in both groups at different time points. (**G**) Quantitative results of the MMP-3^{+} chondrocytes ratio (%) in both groups at different time points. (**H**) A linear regression analysis of the OARSI score with the MMP-3^{+} chondrocytes ratio (%). *$P < 0.05$ and #$P < 0.01$ compared with DDH group. IHC = immunohistochemical; OARSI = Osteoarthritis Research Society International; DDH = developmental dysplasia of the hip; AC = articular cartilage; SB = subchondral bone.

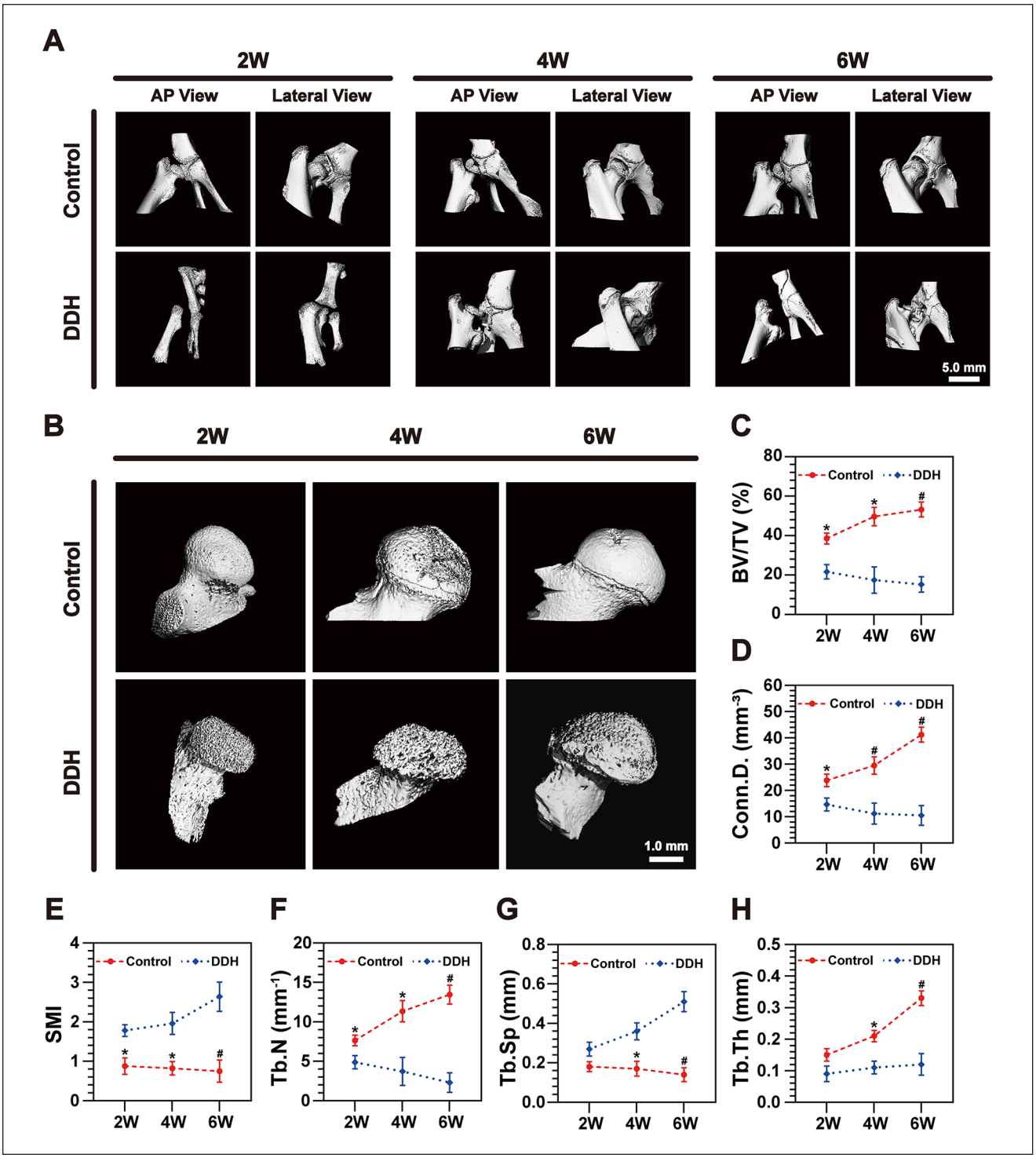

Figure 4. The μCT reconstruction of the hip joint and analysis of subchondral bone microstructural properties at different time points. (**A**) Representative images of the AP and lateral view of the hip joint in both groups. (**B**) Representative images of the femoral head in both groups. (**C-H**) Microstructural analysis of subchondral bone in both groups. μCT = micro–computed tomography; AP = anteroposterior; BV = bone volume; TV = total volume; Conn.D. = connectivity density; SMI = structure model index; Tb.N = trabecular bone number; Tb.Sp = trabecular bone separation; Tb.Th = trabecular bone thickness; DDH = developmental dysplasia of the hip. *$P < 0.05$ compared and #$P < 0.01$ compared with DDH group.

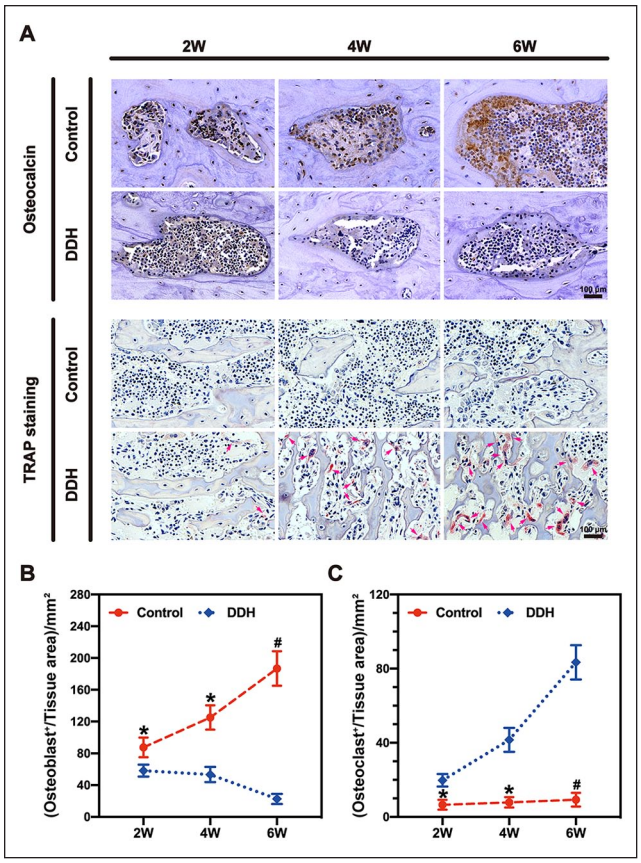

Figure 5. Analysis of the Osteocalcin$^+$ osteoblasts and TRAP$^+$ osteoclasts activity in subchondral bone at different time points. (**A**) IHC staining of Osteocalcin$^+$ osteoblasts and TRAP staining of osteoclasts for subchondral bone in both groups (red arrows indicating the TRAP$^+$ osteoclasts). (**B-C**) Quantitative results of the subchondral bone remodeling cells in both groups. TRAP = tartrate-resistant acid phosphatase; IHC = immunohistochemical; DDH = developmental dysplasia of the hip. *$P < 0.05$ and #$P < 0.01$ compared with DDH group.

during the DDH development. Together, the results of **Tables 1** and **2** indicated that the subchondral bone remodeling activity (especially the abnormal resorption activity) might account for the aberrant subchondral bone changes during the DDH progression, and these subchondral bone changes could likely exacerbate the DDH progress and induce cartilage degradation.

Discussion

In this study, we generated DDH rats using the traditional straight-leg swaddling model to explore the alternations in subchondral trabecular bone microstructural properties and remodeling activity, as well as their correlations with cartilage damage during the DDH progression. We have previously conducted a series of retrospective analyses on patients with advanced DDH and demonstrated that the subchondral bone had undergone many changes and was closely related to the degeneration of overlying cartilage, which eventually induced serious OA symptoms. Moreover, although severe arthritis symptoms may occur in advanced DDH, the specific changes in the remodeling activity and subchondral bone properties were not the same as those of primary OA.[17] In the continuous progression of DDH, the femoral head suffers a long-term dislocation trend and abnormal biomechanical environment, leading to secondary OA in the advanced stage. Prior studies have demonstrated that transformations of subchondral bone acted as a vital role during primary OA, whereas its continuous changes in the time dimension of DDH progression and the effect on secondary cartilage damage remains unknown.[23-26] Therefore, we selected postnatal 2-, 4-, and 6-week DDH rats (according to previous report)[27] to carry out a series of experiments in the present study and found that subchondral bone developed a succession of abnormal remodeling along with DDH exacerbation. Clarifying the relationships between subchondral bone alternations and DDH development could help to elucidate the underlying biomechanisms of this congenital disease. Furthermore, the improvement in subchondral bone with bone-metabolism agents may help mitigate DDH progression.

From our results of macroscopic view, x-ray and μCT reconstructed images, we observed the successfully induced dysplasia hip and typical manifestations of ongoing DDH in rats. Our previous study has demonstrated the imbalance of the biomechanical environment homeostasis occurred in advanced DDH.[17] Owing to a continuous process, the stabilization of biomechanical environment around the femoral head is destined to be gradually broken along with the deterioration of DDH in an age-dependent manner. Considering the relatively greater rigidity and strength than covering cartilage, the subchondral bone bears most of the biomechanical forces transmitted from the joint area.[28] As a matter of fact, the load-bearing capability of subchondral bone, that is, its biomechanical property rely on the microstructure and bone remodeling activities of itself. The positive correlation between microstructure and biomechanical properties in subchondral bone has been proved according to various studies.[16,17,29-33] Aizah *et al.*[34] had originally proposed that significant changes of subchondral bone remodeling occurred at the very early stage in a rat OA model. Although severe OA symptoms appear in the late stage of DDH, the role of subchondral bone in the whole progression of DDH has not been illustrated yet. Our current study showed that though the general view of the hip joint as well as the histological and IHC analysis of cartilage in the DDH group displayed almost no differences with the control group at early stage (2 weeks), the subchondral bone microstructural properties appeared to be inferior, suggesting that alternations in subchondral bone emerged earlier than cartilage degeneration. Moreover, the results indicated that the

Table 1. Correlation Coefficient of Linear Regression between Subchondral Bone Microstructural Properties and Subchondral Bone Remodeling.

Parameter	BV/TV	Conn.D	SMI	Tb.N	Tb.Sp	Tb.Th
Control group						
OCN	0.37*	0.58**	−0.19	0.41*	−0.24	0.63**
TRAP	0.24	0.17	−0.26	0.14	−0.34*	0.17
DDH group						
OCN	0.38*	0.23	−0.42*	0.37*	−0.36*	−0.22
TRAP	−0.35*	−0.34*	0.45*	−0.52**	0.67**	0.18

BV = bone volume; TV = total volume; Conn.D = connectivity density; SMI = structure model index; Tb.N = trabecular bone number; Tb.Sp = trabecular bone separation; Tb.Th = trabecular bone thickness; OCN = osteocalcin; TRAP = tartrate-resistant acid phosphatase; DDH = developmental dysplasia of the hip.
*$P < 0.05$ and **$P < 0.001$ for correlation coefficient.

Table 2. Correlation Coefficient of Linear Regression between Subchondral Bone Microstructural Properties and DDH Severity (Including Articular Cartilage Degeneration).

Parameter	BV/TV	Conn.D	SMI	Tb.N	Tb.Sp	Tb.Th
Control group						
OFA score	0.24	0.17	−0.24	0.19	−0.22	0.08
LCE angle	0.11	0.13	−0.27	0.15	−0.34*	0.14
FC percent	0.33*	0.19	−0.34*	0.41*	−0.54**	0.18
MMP-3	0.09	0.14	−0.25	0.17	−0.22	0.08
DDH group						
OFA score	−0.37*	−0.28	0.33*	−0.57**	0.42*	0.14
LCE angle	0.44*	0.34*	−0.31*	0.42*	−0.36*	−0.26
FC percent	0.43*	0.38*	−0.37*	0.53**	−0.45*	−0.21
MMP-3	−0.35*	−0.37*	0.39*	−0.48*	0.41*	0.12

BV = bone volume; TV = total volume; Conn.D = connectivity density; SMI = structure model index; Tb.N = trabecular bone number; Tb.Sp = trabecular bone separation; Tb.Th = trabecular bone thickness; OFA = Orthopedic Foundation for Animals Hip; LCE angle = lateral center-edge angle; FC percent = femoral coverage percent; MMP-3 = matrix metalloproteinase-3; DDH = developmental dysplasia of the hip.
*$P < 0.05$ and **$P < 0.001$ for correlation coefficient.

peak period of progression was from weeks 4 to 6 and was consistent with the period of accelerated deterioration of subchondral bone microstructural properties, suggesting that the alternation of subchondral bone is the key factor in the acceleration of DDH development. The multiple linear regression analysis showed these subchondral bone changes could give reasons for the aggravating cartilage damage in different stages.

Subchondral bone constantly undergoes dynamic changes of bone resorption and formation, and the precise harmony between osteoclasts and osteoblasts is crucial for maintaining metabolite homeostasis.[35-37] Our previous studies have demonstrated that abnormal bone remodeling could occur once the equilibrium of osteoclasts and osteoblasts was broken, resulting in exacerbation of the subchondral bone, and eventually leading to severe arthritis manifestations.[16,17,30,33] In the current study, the abnormal remodeling in DDH rat subchondral bone has also been observed at the cellular level as relatively active osteoclast activity and sluggish osteoblast activity throughout the disease progression. Furthermore, linear regression analysis revealed that the abnormal remodeling issue was highly correlated with the deteriorated microstructural properties of subchondral bone. We believe that in the initial stage of DDH, the unstable biomechanical condition around malformed hip joint leads to abnormal subchondral bone remodeling, which emerges in the early stage and results in the accelerated aggravation of microstructure and serious degeneration of articular cartilage in the middle and late stages. Indeed, the alliance between subchondral bone microstructural properties and DDH severity was also proved by linear regression analysis, implying the disease progression was based on the incremental deteriorative subchondral bone suffered from abnormal bone remodeling.

Based on the theories in our previous and present results, we illuminated time-dimensional changes in the subchondral bone during the development of DDH and how these changes contribute to disease progression and exacerbation (**Fig. 6**). In the initial stage, preliminary dearticulation arises in the hip joint, which induces the unstable biomechanical environment

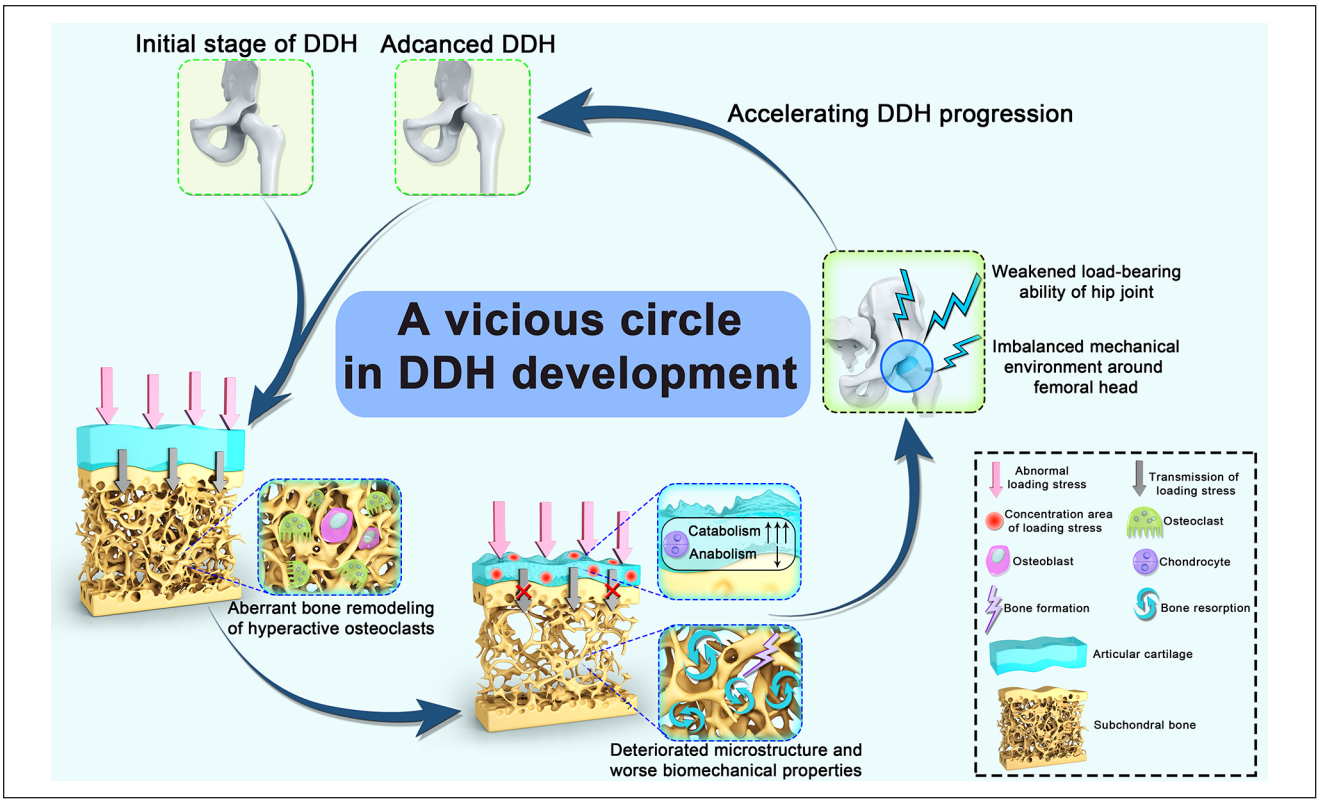

Figure 6. Schematic picture for the potential vicious circle in DDH development. At the initial stage of DDH, the femoral head suffers abnormal loading stress due to the congenital hip joint dearticulation, which leads to the aberrant bone remodeling of hyperactive osteoclasts in the subchondral bone. The predominant bone resorption activity in subchondral bone could account for the deteriorated microstructure and worse biomechanical properties, which restrains the stress transmission from the articular cartilage to the subchondral bone. Thus, the enhanced loading stress concentration on the cartilage layer could disrupt the cartilage metabolic homeostasis. These changes are responsible for the aggravated dislocation and weakened load-bearing ability of the hip joint, as well as imbalanced mechanical environment around the femoral head, therefore forming a vicious circle and consequently accelerating DDH progression. DDH = developmental dysplasia of the hip.

around the femoral head. So far, numerous studies have pointed out that mechanical loading affects the bone mass via regulation of the interactions between bone remodeling cells.[38-41] The femoral head is considered as the main load-bearing structure in the hip joint, and unstable biomechanical stimulation can promote the abnormal activity of osteoclasts and osteoblasts in the subchondral bone, subsequently causing aberrant bone remodeling. With the continuous progress of DDH, the 3-dimensional trabecular bone structure and biomechanical properties of subchondral bone are becoming inferior and worsening. Hence, the weightbearing ability of the subchondral bone is bound to decrease stepwise, leading to unbalanced and abnormal loading stress focusing on the cartilage layer. These changes are responsible for the degeneration of cartilage, appearance of arthritis, and further aggravation of the femoral head malposition as well as the even worse biomechanical environment, and finally forming a vicious circle. The specific vicious circle persists and intensifies over the disease development, which may account for the accelerated pace of secondary OA and late-stage DDH symptoms.

Several limitations in this study need to be declared. First, the investigation should be ideally performed on *in vivo* evaluations of patients in different DDH stages rather than rat models. Actually, the Xtreme-CT is a favorable technique to realize the visualization and quantitative analysis of the subchondral trabecular bone microstructure in the human body.[42] Second, the current study lacks the molecular biological mechanism underlying aberrant subchondral bone remodeling in DDH development. Our further study is dedicating to reveal the precise mechanism at cellular level. Third, due to the unclear etiology of DDH, our conclusions should be limited to the specific model for DDH used here and could not be expanded to all DDH cases in human patients.

Collectively, our study indicates that over the whole DDH progression, the subchondral trabecular bone suffers aberrant bone remodeling activity, deteriorative microstructure, and biomechanical properties that give reasons for the gradual degeneration of overlying cartilage and advanced DDH. As far as we know, this is the first study to elucidate

the biomechanical causality between subchondral bone and articular cartilage during the development of DDH. These findings highlight an innovative target for the prevention and medication of DDH.

Author Contributions

TY, LC, BZ, and ZY were involved in the study design, data collection, and analysis. TY and FX performed animal experiment and drafted the first manuscript. HH, ZH, and MW contributed to data acquisition, interpretation, and experimental suggestions. LC, BZ, and ZY provided funding to support the study. ZY and BZ were involved in the manuscript revising. All the authors have read and approved the submitted manuscript.

Acknowledgments and Funding

The author(s) disclosed receipt of the following financial support for the research, authorship, and/or publication of this article: This work was sponsored by the Youth Program of National Natural Science Foundation of China (No. 32000926), Shanghai Sailing Program (No. 20YF1435600), and the National Natural Science Foundation of China (No. 81870972).

Declaration of Conflicting Interests

The author(s) declared no potential conflicts of interest with respect to the research, authorship, and/or publication of this article.

Ethical Approval

This study was approved by the Institutional Animal Care and Use Committee (IACUC) of Shanghai Jiao Tong University Affiliated Sixth People's Hospital (approval code: SYXK [Shanghai, China] 2020-0072).

ORCID iD

Linyang Chu https://orcid.org/0000-0001-9585-2967

References

1. Gala L, Clohisy JC, Beaulé PE. Hip dysplasia in the young adult. J Bone Joint Surg Am. 2016;98(1):63-73. doi:10.2106/jbjs.O.00109.
2. Cheng B, Jia Y, Wen Y, Hou W, Xu K, Liang C, *et al*. Integrative analysis of MicroRNA and mRNA sequencing data identifies novel candidate genes and pathways for developmental dysplasia of hip. Cartilage. 2021;13(Suppl 2):1618S-1626S. doi:10.1177/1947603521990859.
3. Xu J, Li D, Ma RF, Barden B, Ding Y. Application of rapid prototyping pelvic model for patients with DDH to facilitate arthroplasty planning: a pilot study. J Arthroplasty. 2015;30(11):1963-70. doi:10.1016/j.arth.2015.05.033.
4. Sekimoto T, Ishii M, Emi M, Kurogi S, Funamoto T, Yonezawa Y, *et al*. Copy number loss in the region of the ASPN gene in patients with acetabular dysplasia: ASPN CNV in acetabular dysplasia. Bone Joint Res. 2017;6(7):439-45. doi:10.1302/2046-3758.67.Bjr-2016-0094.R1.
5. Hernandez PA, Wells J, Usheva E, Nakonezny PA, Barati Z, Gonzalez R, *et al*. Early-onset osteoarthritis originates at the chondrocyte level in hip dysplasia. Sci Rep. 2020;10(1):627. doi:10.1038/s41598-020-57431-x.
6. Tian FD, Zhao DW, Wang W, Guo L, Tian SM, Feng A, *et al*. Prevalence of developmental dysplasia of the hip in Chinese adults: a cross-sectional survey. Chin Med J (Engl). 2017;130(11):1261-8. doi:10.4103/0366-6999.206357.
7. Rogers BA, Garbedian S, Kuchinad RA, Backstein D, Safir O, Gross AE. Total hip arthroplasty for adult hip dysplasia. J Bone Joint Surg Am. 2012;94(19):1809-21. doi:10.2106/jbjs.K.00779.
8. Agricola R, Heijboer MP, Roze RH, Reijman M, Bierma-Zeinstra SM, Verhaar JA, *et al*. Pincer deformity does not lead to osteoarthritis of the hip whereas acetabular dysplasia does: acetabular coverage and development of osteoarthritis in a nationwide prospective cohort study (CHECK). Osteoarthritis Cartilage. 2013;21(10):1514-21. doi:10.1016/j.joca.2013.07.004.
9. Clement ND, Gaston P, Bell A, Simpson P, Macpherson G, Hamilton DF, *et al*. Robotic arm-assisted versus manual total hip arthroplasty. Bone Joint Res. 2021;10(1):22-30. doi:10.1302/2046-3758.101.Bjr-2020-0161.R1.
10. Zhu J, Chen X, Cui Y, Shen C, Cai G. Mid-term results of Bernese periacetabular osteotomy for developmental dysplasia of hip in middle aged patients. Int Orthop. 2013;37(4):589-94. doi:10.1007/s00264-013-1790-z.
11. Chen Y, Hu Y, Yu YE, Zhang X, Watts T, Zhou B, *et al*. Subchondral trabecular rod loss and plate thickening in the development of osteoarthritis. J Bone Miner Res. 2018;33(2):316-27. doi:10.1002/jbmr.3313.
12. Liu C, Liu C, Si L, Shen H, Wang Q, Yao W. Relationship between subchondral bone microstructure and articular cartilage in the osteoarthritic knee using 3T MRI. J Magn Reson Imaging. 2018;48(3):669-79. doi:10.1002/jmri.25982.
13. Chen L, Hong G, Fang B, Zhou G, Han X, Guan T, *et al*. Predicting the collapse of the femoral head due to osteonecrosis: from basic methods to application prospects. J Orthop Translat. 2017;11:62-72. doi:10.1016/j.jot.2016.11.002.
14. Nakahata A, Ito A, Nakahara R, Kishimoto A, Imaizumi A, Hashimoto T, *et al*. Intra-articular injections of curcumin monoglucuronide TBP1901 suppresses articular cartilage damage and regulates subchondral bone alteration in an osteoarthritis rat model. Cartilage. 2021;13(Suppl 2):153S-167S. doi:10.1177/19476035211043202.
15. Liu XS, Sajda P, Saha PK, Wehrli FW, Guo XE. Quantification of the roles of trabecular microarchitecture and trabecular type in determining the elastic modulus of human trabecular bone. J Bone Miner Res. 2006;21(10):1608-17. doi:10.1359/jbmr.060716.
16. Chu L, Liu X, He Z, Han X, Yan M, Qu X, *et al*. Articular cartilage degradation and aberrant subchondral bone remodeling in patients with osteoarthritis and osteoporosis. J Bone Miner Res. 2020;35(3):505-15. doi:10.1002/jbmr.3909.
17. Chu L, He Z, Qu X, Liu X, Zhang W, Zhang S, *et al*. Different subchondral trabecular bone microstructure and biomechanical properties between developmental dysplasia of the hip and primary osteoarthritis. J Orthop Translat. 2020;22:50-7. doi:10.1016/j.jot.2019.09.001.

18. Wang E, Liu T, Li J, Edmonds EW, Zhao Q, Zhang L, *et al*. Does swaddling influence developmental dysplasia of the hip? An experimental study of the traditional straight-leg swaddling model in neonatal rats. J Bone Joint Surg Am. 2012;94(12):1071-7. doi:10.2106/jbjs.K.00720.
19. Bo N, Peng W, Xinghong P, Ma R. Early cartilage degeneration in a rat experimental model of developmental dysplasia of the hip. Connect Tissue Res. 2012;53(6):513-20. doi:10.3109/03008207.2012.700346.
20. Pascual-Garrido C, Guilak F, Rai MF, Harris MD, Lopez MJ, Todhunter RJ, *et al*. Canine hip dysplasia: a natural animal model for human developmental dysplasia of the hip. J Orthop Res. 2018;36(7):1807-17. doi:10.1002/jor.23828.
21. Pritzker KP, Gay S, Jimenez SA, Ostergaard K, Pelletier JP, Revell PA, *et al*. Osteoarthritis cartilage histopathology: grading and staging. Osteoarthritis Cartilage. 2006;14(1):13-29. doi:10.1016/j.joca.2005.07.014.
22. Reagan JK. Canine hip dysplasia screening within the United States: Pennsylvania hip improvement program and orthopedic foundation for animals hip/elbow database. Vet Clin North Am Small Anim Pract. 2017;47(4):795-805. doi:10.1016/j.cvsm.2017.02.003.
23. Kadri A, Funck-Brentano T, Lin H, Ea HK, Hannouche D, Marty C, *et al*. Inhibition of bone resorption blunts osteoarthritis in mice with high bone remodelling. Ann Rheum Dis. 2010;69(8):1533-8. doi:10.1136/ard.2009.124586.
24. Li G, Yin J, Gao J, Cheng TS, Pavlos NJ, Zhang C, *et al*. Subchondral bone in osteoarthritis: insight into risk factors and microstructural changes. Arthritis Res Ther. 2013;15(6):223. doi:10.1186/ar4405.
25. Adebayo OO, Ko FC, Wan PT, Goldring SR, Goldring MB, Wright TM, *et al*. Role of subchondral bone properties and changes in development of load-induced osteoarthritis in mice. Osteoarthritis Cartilage. 2017;25(12):2108-18. doi:10.1016/j.joca.2017.08.016.
26. Kroker A, Bhatla JL, Emery CA, Manske SL, Boyd SK. Subchondral bone microarchitecture in ACL reconstructed knees of young women: a comparison with contralateral and uninjured control knees. Bone. 2018;111:1-8. doi:10.1016/j.bone.2018.03.006.
27. Fu M, Liu J, Huang G, Huang Z, Zhang Z, Wu P, *et al*. Impaired ossification coupled with accelerated cartilage degeneration in developmental dysplasia of the hip: evidences from μCT arthrography in a rat model. BMC Musculoskelet Disord. 2014;15:339. doi:10.1186/1471-2474-15-339.
28. Zhen G, Cao X. Targeting TGFβ signaling in subchondral bone and articular cartilage homeostasis. Trends Pharmacol Sci. 2014;35(5):227-36. doi:10.1016/j.tips.2014.03.005.
29. Chen Y, Huang YC, Yan CH, Chiu KY, Wei Q, Zhao J, *et al*. Abnormal subchondral bone remodeling and its association with articular cartilage degradation in knees of type 2 diabetes patients. Bone Res. 2017;5:17034. doi:10.1038/boneres.2017.34.
30. He Z, Chu L, Liu X, Han X, Zhang K, Yan M, *et al*. Differences in subchondral trabecular bone microstructure and finite element analysis-based biomechanical properties between osteoporosis and osteoarthritis. J Orthop Translat. 2020;24:39-45. doi:10.1016/j.jot.2020.05.006.
31. Liu XS, Zhang XH, Sekhon KK, Adams MF, McMahon DJ, Bilezikian JP, *et al*. High-resolution peripheral quantitative computed tomography can assess microstructural and mechanical properties of human distal tibial bone. J Bone Miner Res. 2010;25(4):746-56. doi:10.1359/jbmr.090822.
32. Zhen G, Guo Q, Li Y, Wu C, Zhu S, Wang R, *et al*. Mechanical stress determines the configuration of TGFβ activation in articular cartilage. Nat Commun. 2021;12(1):1706. doi:10.1038/s41467-021-21948-0.
33. Zhou F, Chu L, Liu X, He Z, Han X, Yan M, *et al*. Subchondral trabecular microstructure and articular cartilage damage variations between osteoarthritis and osteoporotic osteoarthritis: a cross-sectional cohort study. Front Med (Lausanne). 2021;8:617200. doi:10.3389/fmed.2021.617200.
34. Aizah N, Chong PP, Kamarul T. Early alterations of subchondral bone in the rat anterior cruciate ligament transection model of osteoarthritis. Cartilage. 2021;13:1322S-1333S. doi:10.1177/1947603519878479.
35. Hu W, Chen Y, Dou C, Dong S. Microenvironment in subchondral bone: predominant regulator for the treatment of osteoarthritis. Ann Rheum Dis. 2020;80:413-22. doi:10.1136/annrheumdis-2020-218089.
36. Zhu X, Chan YT, Yung PSH, Tuan RS, Jiang Y. Subchondral bone remodeling: a therapeutic target for osteoarthritis. Front Cell Dev Biol. 2020;8:607764. doi:10.3389/fcell.2020.607764.
37. Tang Y, Wu X, Lei W, Pang L, Wan C, Shi Z, *et al*. TGF-beta1-induced migration of bone mesenchymal stem cells couples bone resorption with formation. Nat Med. 2009;15(7):757-65. doi:10.1038/nm.1979.
38. Meakin LB, Galea GL, Sugiyama T, Lanyon LE, Price JS. Age-related impairment of bones' adaptive response to loading in mice is associated with sex-related deficiencies in osteoblasts but no change in osteocytes. J Bone Miner Res. 2014;29(8):1859-71. doi:10.1002/jbmr.2222.
39. Klein-Nulend J, Bacabac RG, Bakker AD. Mechanical loading and how it affects bone cells: the role of the osteocyte cytoskeleton in maintaining our skeleton. Eur Cell Mater. 2012;24:278-91. doi:10.22203/ecm.v024a20.
40. Klein-Nulend J, Bakker AD, Bacabac RG, Vatsa A, Weinbaum S. Mechanosensation and transduction in osteocytes. Bone. 2013;54(2):182-90. doi:10.1016/j.bone.2012.10.013.
41. Bonewald LF. The amazing osteocyte. J Bone Miner Res. 2011;26(2):229-38. doi:10.1002/jbmr.320.
42. Kroker A, Zhu Y, Manske SL, Barber R, Mohtadi N, Boyd SK. Quantitative in vivo assessment of bone microarchitecture in the human knee using HR-pQCT. Bone. 2017;97:43-8. doi:10.1016/j.bone.2016.12.015.